Pileup shocks to cause the red-aurora magnetic storm on November 4-6, 2023

Ryuho Kataoka[1,2] and Yumi Bamba[3]

[1]National Institute of Polar Research

[2]SOKENDAI

[3]National Institute of Information and Communications Technology

Corresponding author: Ryuho Kataoka (kataoka.ryuho@nipr.ac.jp)

Keywords: Interplanetary shock, coronal mass ejection, magnetic storm, space weather

Key Points:

- We analyzed the in-situ solar wind data of the glancing blows of three interplanetary shocks on November 4-6, 2023.
- We identified that the shock pileup region caused the unexpectedly large multi-step magnetic storm.
- We suggest that the storm recovery was prolonged by lasagna-like remnant structure associated with the shock pileup.

Abstract

Glancing blows of three interplanetary shocks caused an unexpectedly large magnetic storm on November 4-6, 2023, which was popular for citizen scientists because of the surprising appearance of the crimson-red auroras world-wide in middle latitudes. Based on the analysis of the in-situ interplanetary magnetic field data observed at closely located DSCOVR and STEREO-A, we show that the multi-step main phase of the magnetic storm is explained by the shock pileup, i.e. slow interplanetary shock was caught up from behind by the fast one, and the multi-step prolonged recovery phase can be explained by the remnant structure associated with the shock pileup.

Plain Language Summary

In the modern high-tech society, the importance of predicting magnetic storms is growing and the high-resolution understanding of the minor and dirty solar wind structures rather than the textbook picture of beautiful shock-ejecta pair is the urgent issue. We identified that both shock pileup and the remnant structure are important to evaluate the geo-effectiveness of the glancing blows of interplanetary shock waves, and to forecast the start and the end of the relevant magnetic storms especially associated with partial-halo coronal mass ejections.

1 Introduction

It is important to understand the mechanisms to form the strong southward directing interplanetary magnetic field (IMF) to predict both the start and the end of magnetic storms. The standard picture to cause the SBZ (southward-directing IMF) is the shock-downstream SBZ and/or following magnetic-cloud SBZ (Tsurutani et al., 1998; Kataoka and Miyoshi, 2006), although such a standard picture is not always applicable to many space weather events.

The shock downstream structures have been investigated in detail by Kataoka et al. (2005) as one of the major drivers of intense magnetic storms and concluded that the planar magnetic structure (PMS; Nakagawa et al., 1989, Jones et al., 2002) caused by the shock compression of the ambient solar wind structures is a plausible mechanism. However, in this modern high-tech society, the importance of higher-resolution understanding of the other geoeffective structures is growing to predict the actual SBZ pattern. For example, moderate magnetic storms in February 2022 caused the atmospheric reentry of more than 38 Starlink satellites (Hapgood et al., 2022; Kataoka et al., 2022), and notified us the importance of the understanding of the start and the end of minor magnetic storms as driven by non-direct hits of ejecta, such as related to the flank-side of coronal mass ejections (CMEs) or only glancing blows of interplanetary shocks.

An unexpectedly large-amplitude magnetic storm occurred on Nov. 4-6, 2023, reaching the minimum quick-look Dst index of -165 nT at 19-20 UT on Nov. 5. The strong SBZ in the shock downstream (therefore very high density as well) continues for more than 5 hours from 14 UT to19 UT to drive the storm main phase. This magnetic storm was popular because of many surprising witness records of crimson-red auroras world-wide in middle latitudes, including the one from Rikubetsu, Hokkaido, Japan at 36.8 deg. magnetic latitude (L=1.6), as concurrently occurred with geosynchronous magnetopause crossing (GMC) at 15-18 UT, although only C-class flares occurred at that time. This situation reminded us of the unexpectedly large magnetic storm on March 17, 2015 when the Japan aurora occurred with the GMC associated with C-class flares (Kataoka et al., 2015; Bamba et al. 2019).

Somewhat unique characteristics of this Nov. 4-6, 2023 magnetic storm is the multi-step main phase and multi-step recovery phase. The cause of the multi-step main phase is obvious. We can easily identify the shock-downstream SBZ pattern associated with multiple interplanetary shocks which arrived at 1 AU at close timing, as explained later in detail in Section 2. The enhanced SBZ disturbance is naturally expected because in general the magnetic field intensities and density associated with the shock interaction or multiple shocks will be higher than those associated with the isolated one.

In contrast, the cause of multi-step recovery phase is not obvious. The multiple SBZ portions in the trailing part of this Nov. 4-6 storm event looked as if repeatedly appeared mini flux ropes that were separated by directional discontinuities (DDs), that is why we call the structure as “lasagna” in this paper. The lasagna structure has not been discussed in literature to the authors knowledge probably because they are just a minor sub-structure associated with CMEs. We will discuss the cause of the lasagna structure in detail later in Section 2 and 3.

Such a complex solar wind structure is far from the standard text-book picture of shock-cloud pair (e.g., Kataoka and Miyoshi, 2006), and sometimes classified as the complex ejecta (Burlaga et al. 2001; 2002). Lugaz and Farrugia (2014), for example, successfully explained the basic characteristics of the complex ejecta, such as short duration of the first CME and the longer tail than a single CME event, by conducting the magenetohydrodynamic (MHD) simulation of interacting CMEs. In this paper, we take a different approach to untangle a part of the complex solar wind structures causing the Nov 4-6 magnetic storm event. We propose a new subcategory of the geoeffective glancing blows without ejecta, where the shock pileup region and the remnant structure associated with the shock pileup can explain the start and the end of magnetic storms, respectively.

2 Event overview

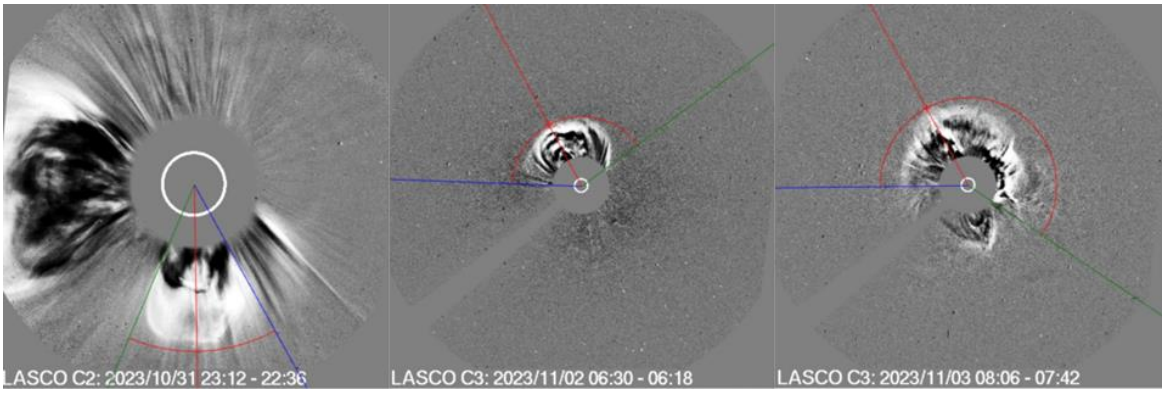

Figure 1. CME0 (left), CME1 (middle), and CME2 (right) which caused the Nov. 4-6, 2023 magnetic storm. The CME speeds are estimated to be 580 km s^{-1}, 550 km s^{-1}, and 780 km s^{-1}, respectively, using the NICT forecast tool (Shiota and Yashiro, 2021).

All of the filament eruptions and CMEs as shown in **Figure 1** were associated with only C-class flares. The first arrival of the DD (downstream speed is ~300 km s^{-1}), as denoted by DD0 in **Figures 2 and 3**, were observed by DSCOVR and STEREO-A at ~1200 UT on Nov. 4. Note that both spacecraft are located at ~1 AU distance from the Sun, and close to the Earth position in the inner heliosphere. The DD0 can be associated with the filament eruption at ~2200 UT on Oct. 31 occurred around AR13474 in the Sun's southern hemisphere. The related CME (CME0) went to the south with a speed of ~580 km s^{-1}. First of all, the "pre-conditioning" made by the CME0 was important to make the background magnetic field higher than usual.

The origins of the shock 1 (downstream speed and density are ~400 km s^{-1} and >20 /cc), and shock 2 (downstream speed and density are ~500 km s^{-1} and >40 /cc), as denoted by S1 and S2 in **Figures 2 and 3**, are identified to be the partial-halo CMEs; the first CME (CME 1) was associated with the filament eruption at 0300 UT on Nov. 2 in the northern and eastern hemispheres, launching toward the north-east at ~550 km s^{-1}, while the second CME (CME 2) was associated with the filament eruption at ~0500 UT on Nov. 3 occurred between AR13472 and AR13473 in the norther and western hemispheres, launching toward the north-west at ~780 km s^{-1}. We expected only the glancing blows of the CME-related shocks without direct hits of the ejecta, i.e., no flux-rope arrivals expected, because they are partial-halo CMEs lanched from off-center active regions. It was anticipated, however, that the fast CME 2 could catch up the slow CME 1 at ~1 AU. In this paper, we call the catching-up shock region as the "shock pileup" region.

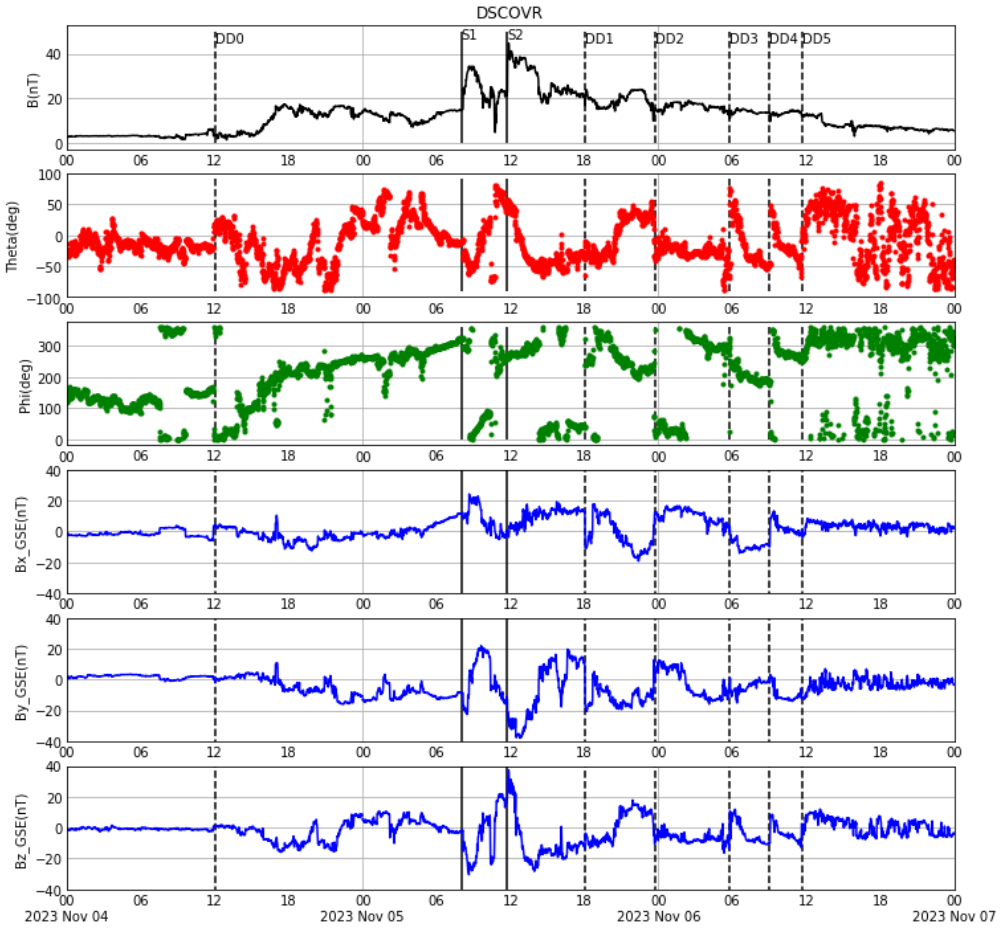

Figure 2. DSCOVR magnetic field data. The spacecraft location is GSE (x, y, z) = (243, -10, 25) R_E. Shocks and directional discontinuities are marked by solid and dashed lines, respectively. Theta is latitude angle, while Phi is the azimuth angle measured from the GSE X axis.

The weird "lasagna" structure appeared at DSCOVR position, as denoted from DD2 to DD5 in **Figure 2**. Such an echoing mini flux rope-like magnetic-field rotations cannot be explained by the standard text-book picture of the CME-related flux rope. As shown in **Figure 3**, the lasagna structure is less clear at STEREO-A position where the magnetic field amplitudes around the shocks 1 and 2 are weaker and the distance between shocks 1 and 2 are larger, compared to those at DSCOVR. From these differences between DSCOVR and STEREO-A, we will discuss later in Section 3 that the appearance and disappearance of the lasagna structure can be associated with the evolving and less-evolving shock pileup regions.

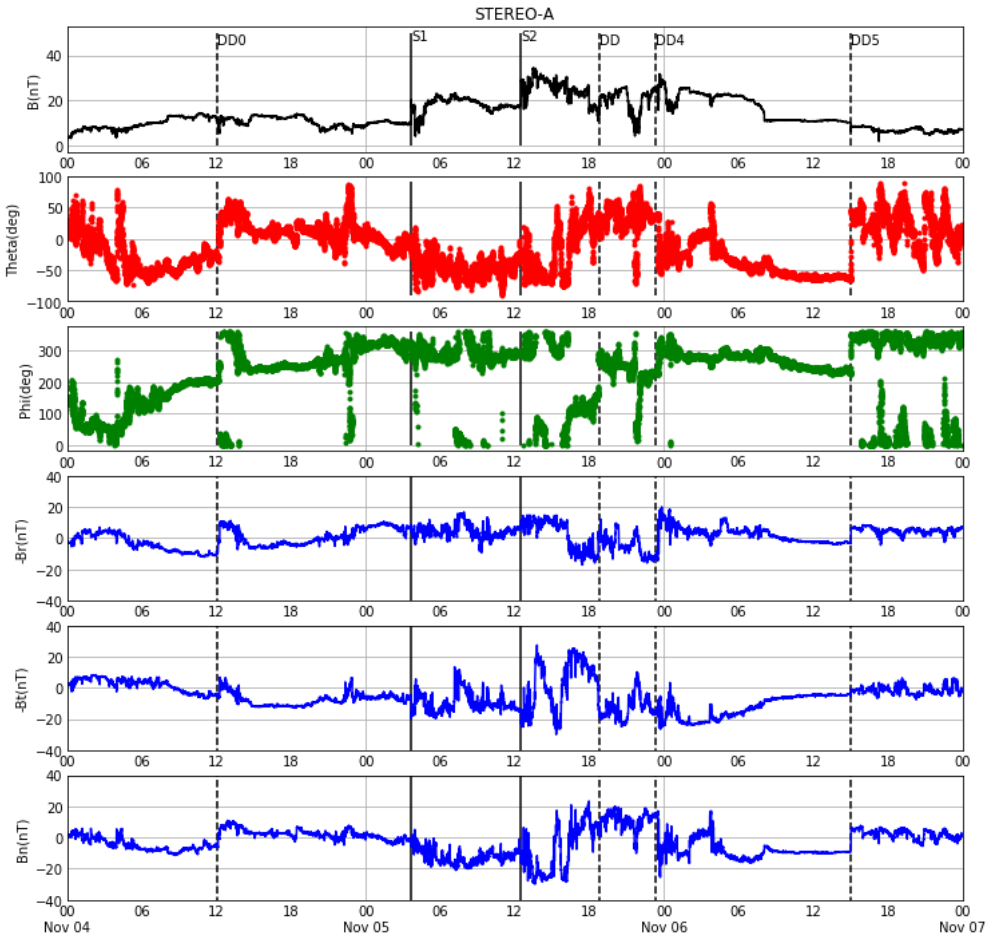

Figure 3. STEREO-A magnetic field data. The spacecraft location is GSE (x, y, z) = (741, -2267, -12) R_E. Shocks and directional discontinuities are marked by solid and dashed lines, respectively. Note that we plotted -Br, -Bt, Bn components to mimic the GSE X, Y, and Z components.

3 Results and Discussions

In this Section, we first apply the minimum variance analysis (MVA) to see the expected PMS nature in the shock pileup region. We also check if the magnetic field fluctuation of the trailing lasagna structure followed the PMS nature. Then we apply the helical decomposition analysis to examine the sense of IMF rotation polarities of the PMS and the lasagna structure. The IDL procedures to do the data analysis are publicly available at GitHub (https://github.com/ryuhokataoka/TOOLS).

In general, from the MVA of the fluctuating magnetic field, we can find the minimum variance plane with the normal vector with its smallest eigenvalue (Sonnerup and Carhill, 1967). We applied the same MVA method as done by Kataoka et al. (2015), to the shock pileup region, including the two shocks. We take the shock pileup region as the high-density region until 2400 UT on Nov. 5. The proton density becomes smaller thereafter.

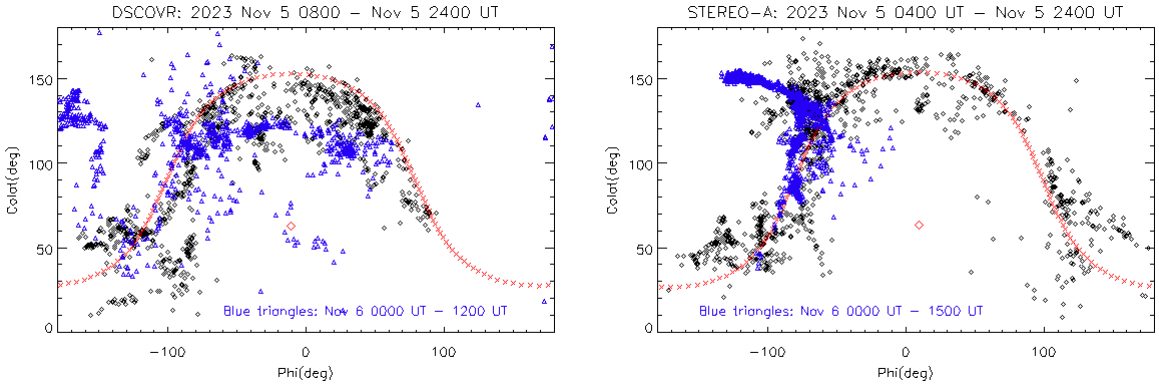

Figure 4. MVA planes (red crosses) and the MVA normal vectors (red diamonds) for DSCOVR (left) and STEREO-A (right), including the shocks in the shock pileup region. The vertical and horizontal axes are colatitude and azimuth angles of the IMF, respectively. Blue triangles show the IMF directions in the trailing lasagna structure.

As shown in **Figure 4**, it is found that magnetic field vectors in the shock pileup region roughly aligned in the MVA planes at both DSCOVR and STEREO-A, i.e., very similar PMS structures can be found at both DSCOVR and STEREO-A. The north-south inclinations of the MVA planes are consistent with the northward directing CMEs (partial-halo CME 1 and CME 2), although the east-west inclinations of the MVA planes are not clear, almost flat against the Sun-Earth line. From the MVA result, we can conclude that a subset of PMS is the shock pileup region where slower shock was caught up from behind by the faster shock.

The magnetic field directions of the lasagna structure are also shown by blue triangles in **Figure 4**. It is clear that the lasagna structure has very different IMF directions from the PMS at DSCOVR, while at STEREO-A the IMF directions partly follow and then gradually deviate from the PMS.

The fluctuating magnetic field data can also be separated into positive and negative helical parts (Terasawa et al., 1986). The advanced version of such a helical decomposition analysis can be done by the one-dimensional S-transform (Stockwell et al., 1996; 2004), inputting a one-dimensional complex-valued time series. More specifically, by putting By and Bz components of DSCOVR (-Br and -Bt components for STEREO-A) in the real and imaginary parts, respectively, we use the S-transform relative amplitudes of the positive and negative frequency to see the sense of polarity (Kataoka et al., 2009). Here we roughly assumed the axis as X direction, considering that both satellites sit approximately in the Toward IMF sector during the whole interval (**Figures 2 and 3**).

It is found from **Figure 5** that the shock pileup region before 2400 UT on Nov. 5 has the larger amplitude in the positive frequency than the negative one, while the trailing structure after 24 UT on Nov. 5, including the lasagna structure at DSCOVR, has the amplitude dominantly in the negative frequency. The amplitude and the extent of the trailing part in the negative frequency spectra are weaker at STEREO-A than those at DSCOVR, which can also be interpreted by the idea that the pileup evolution was weaker at STEREO-A location, as seen from the relatively large distance between shocks 1 and 2, and the remnant lasagna was not fully

181 developed yet at STEREO-A position. Toward the next-generation space weather forecasting, we
182 hope to stimulate MHD modelers to investigate how to reconstruct the trailing lasagna structure
183 with the reverse polarity of the PMS body, with some variations associated with the evolution
184 stage of the pile-up PMS.

185

186

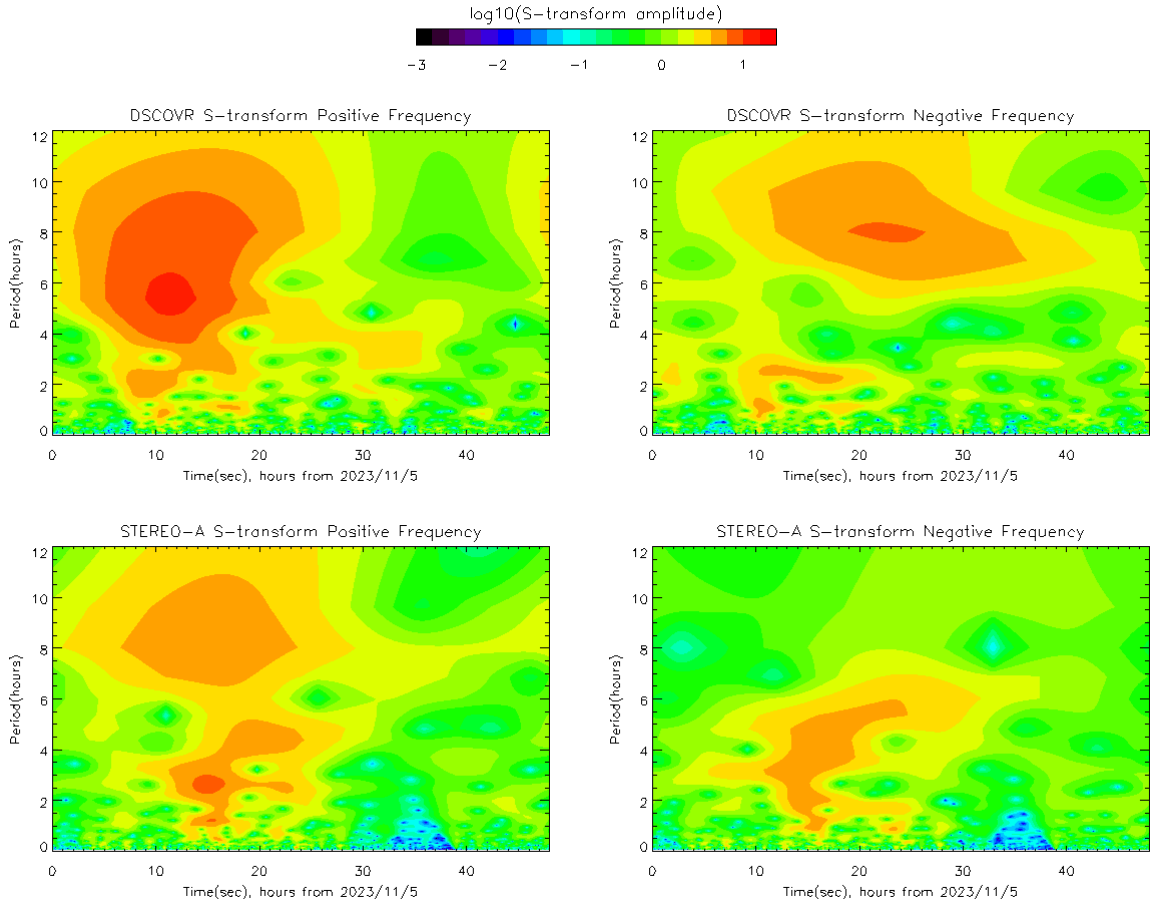

187

188

189 **Figure 5**. Helical decomposition analysis by the S-transform. DSCOVR (top) and STEREO-A
190 (bottom). S-transform amplitude for both positive (left) and negative (right) frequencies are
191 shown to see the polarity changes.

192

193 **4 Summary**

194 We showed an example that the glancing blows of multiple interplanetary shocks can be
195 geoeffective to cause the main phase of a large magnetic storm on Nov. 4-6, 2023, under the
196 condition that the low-speed and high-speed shocks arrived together at close timing at 1 AU to
197 form the PMS, with the help of preconditioning to pave the strong background magnetic field in
198 advance. Further, based on the helical decomposition analysis, we showed that the lasagna-like
199 trailing remnant structure had a reverse sense of the IMF polarity with the associated shock-
200 pileup PMS, which prolonged the recovery time of the magnetic storm.

This study suggests that the shock-pileup PMS and the trailing lasagna-like remnant of the PMS formation are the origins of the complex SBZ pattern which contributed to the multi-step main phase and multi-step recovery phase of the large magnetic storm, respectively. The deterministic prediction of such a complex SBZ pattern is therefore not an easy task. Rather, in future, it would be essential and important to understand the basic properties of the ambient low-frequency IMF turbulence in the solar wind, and to develop the statical and/or probabilistic ways to predict the complex SBZ pattern as created by the nonlinear shock pileup process.

Acknowledgments

We acknowledge the data use of SOHO, DSCOVR, and STEREO-A. The SOHO/LASCO data used here are produced by a consortium of the Naval Research Laboratory (USA), Max-Planck-Institut fuer Aeronomie (Germany), Laboratoire d'Astronomie (France), and the University of Birmingham (UK).

Open Research

DSCOVR Magnetometer m1m data (*_pub.nc) can be obtained from the NOAA website (https://www.ngdc.noaa.gov/dscovr/portal/index.html). STEREO-A Magnetometer data (*V02.cdf) can be obtained from the NASA website (https://stereo-ssc.nascom.nasa.gov/data/beacon/ahead/impact/2023/11/). All of the IDL procedures used for the magnetic field data analysis are available at https://github.com/ryuhokataoka/TOOLS (DOI:10.5281/zenodo.10212082).

References

Bamba, Y., Inoue, S., Hayashi, K. (2019), The Role of a Tiny Brightening in a Huge Geoeffective Solar Eruption Leading to the St. Patrick's Day Storm, The Astrophysical Journal, 874:73 (11pp), doi:10.3847/1538-4357/ab06ff.

228 Burlaga, L. F., Behannon, K. W., and Klein, L. W. (1987), Compound streams, magnetic clouds,
229 and major geomagnetic storms, J. Geophys. Res., 92(A6), 5725-5734,
230 doi:10.1029/JA092iA06p05725.
231
232 Burlaga, L. F., Skoug, R. M., Smith, C. W., Webb, D. F., Zurbuchen, T. H., and Reinard, A.
233 (2001), Fast ejecta during the ascending phase of solar cycle 23: ACE observations, 1998-1999,
234 J. Geophys. Res., 106(A10), 20957?20977, doi:10.1029/2000JA000214.
235
236 Burlaga, L. F., Plunkett, S. P., and St. Cyr, O. C., Successive CMEs and complex ejecta, J.
237 Geophys. Res., 107(A10), 1266, doi:10.1029/2001JA000255, 2002.
238
239 Hapgood, M., Liu, H., & Lugaz, N. (2022). SpaceX - Sailing close to the space weather? Space
240 Weather, 20, e2022SW003074. https://doi.org/10.1029/2022SW003074
241
242 Jones, G. H., Rees, A., Balogh, A., and Forsyth, R. J., The draping of heliospheric magnetic
243 fields upstream of coronal mass ejecta, Geophys. Res. Lett., 29(11),
244 doi:10.1029/2001GL014110, 2002.
245
246 Kataoka, R., S. Watari, N. Shimada, H. Shimazu, and K. Marubashi (2005), Downstream
247 structures of interplanetary fast shocks associated with coronal mass ejections, Geophys. Res.
248 Lett., 32, L12103, doi:10.1029/2005GL022777.
249

Kataoka, R., and Y. Miyoshi (2006), Flux enhancement of radiation belt electrons during geomagnetic storms driven by coronal mass ejections and corotating interaction regions, Space Weather, 4, S09004, doi:10.1029/2005SW000211.

Kataoka, R., D. Shiota, E. Kilpua, and K. Keika (2015), Pileup accident hypothesis of magnetic storm on 2015 March 17, Geophys. Res. Lett, 42, 5155-5161, doi:10.1002/2015GL064816.

Kataoka, R., D. Shiota, H. Fujiwara, H. Jin, C. Tao, H. Shinagawa, and Y. Miyoshi (2022), Unexpected space weather causing the reentry of 38 Starlink satellites in February 2022, J. Space Weather and Space Climate, 12, 41, https://doi.org/10.1051/swsc/2022034.

Lugaz, N., and Farrugia, C. J. (2014), A new class of complex ejecta resulting from the interaction of two CMEs and its expected geoeffectiveness, Geophys. Res. Lett., 41, 769-776, doi:10.1002/2013GL058789.

Nakagawa, T., Nishida, A., and Saito, T. (1989), Planar magnetic structures in the solar wind, J. Geophys. Res., 94(A9), 11761-11775, doi:10.1029/JA094iA09p11761.

Shiota D., and S. Yashiro (2021), 4-1. Real-time prediction system for solar storm arrival, NICT Research Report, Vol. 67, No. 1, pp137-142 (in Japanese with English abstract), https://www.nict.go.jp/data/research-report/index.html

Sonnerup, B. U., and Cahill, L. J. (1967), Magnetopause structure and attitude from Explorer 12 observations, J. Geophys. Res., 72(1), 171?183, doi:10.1029/JZ072i001p00171.

Stockwell, R. G., L. Mansinha, and R. P. Lowe (1996), Localization of the complex spectrum: The Stransform, IEEE Trans. Signal Process., 44(4), 998-1001, doi:10.1109/78.492555.

Stockwell, R. G., W. G. Large, and R. F. Milliff (2004), Resonant inertial oscillations in moored buoy ocean surface winds, Tellus, Ser. A, 56(5), 536-547, doi:10.1111/j.1600-0870.2004.00086.x.

Terasawa T., Hoshino M., J.-I. Sakai, and T. Hada (1986), Decay instability of finite-amplitude circularly polarized Aflven waves: A numerical simulation of stimulated Brillouin scattering, J. Geophys. Res., 91, A4, 4171-4187.

Tsurutani, B. T., Gonzalez, W. D., Tang, F., Akasofu, S. I., and Smith, E. J. (1988), Origin of interplanetary southward magnetic fields responsible for major magnetic storms near solar maximum (1978-1979), J. Geophys. Res., 93(A8), 8519-8531, doi:10.1029/JA093iA08p08519.